

# **JGR** Biogeosciences

### RESEARCH ARTICLE

10.1029/2018JG004817

### **Key Points:**

- Ultrahigh-resolution mass spectrometry revealed molecular hysteresis of dissolved organic matter in a forested New England catchment
- Aliphatic compounds were enriched at storm onset, and aromatic compounds were enriched at peak discharge
- Similarities in molecular hysteresis across stream orders suggested event-driven transport of fresh organic material further downstream

**Supporting Information:** 

· Supporting Information S1

Correspondence to: S. Wagner, s.wagner@northeastern.edu

### Citation:

Wagner, S., Fair, J. H., Matt, S., Hosen, J. D., Raymond, P., Saiers, J., et al. (2019). Molecular hysteresis: Hydrologically driven changes in riverine dissolved organic matter chemistry during a storm event. *Journal of Geophysical Research: Biogeosciences*, 124. https://doi.org/10.1029/2018JG004817

Received 18 SEP 2018 Accepted 24 FEB 2019 Accepted article online 5 MAR 2019

## Molecular Hysteresis: Hydrologically Driven Changes in Riverine Dissolved Organic Matter Chemistry during a Storm Event

Sasha Wagner<sup>1</sup>, Jennifer Hoyle Fair<sup>2,3</sup>, Serena Matt<sup>2</sup>, Jacob D. Hosen<sup>2,4</sup>, Peter Raymond<sup>2</sup>, James Saiers<sup>2</sup>, James B. Shanley<sup>5</sup>, Thorsten Dittmar<sup>6</sup>, and Aron Stubbins<sup>1</sup>

<sup>1</sup>Departments of Marine and Environmental Sciences, Civil and Environmental Engineering, and Chemistry and Chemistry and Chemical Biology, Northeastern University, Boston, MA, USA, <sup>2</sup>School of Forestry and Environmental Studies, Yale University, New Haven, CT, USA, <sup>3</sup>Now at U.S. Geological Survey, Northborough, MA, USA, <sup>4</sup>U.S. Geological Survey, Montpelier, VT, USA, <sup>5</sup>Now at School of Forest Resources and Conservation, University of Florida, Gainesville, FL, USA, <sup>6</sup>Research Group for Marine Geochemistry (ICBM-MPI Bridging Group), Institute for Chemistry and Biology of the Marine Environment, Carl von Ossietzky University of Oldenburg, Oldenburg, Germany

Abstract Hydrological events, driven by rainfall, control the amount and composition of dissolved organic matter (DOM) mobilized through river networks. In forested watersheds, the concentration, composition, and reactivity of DOM exported changes as baseflow transitions to storm flow, with major implications to downstream biogeochemistry. Hysteresis describes an observed difference between in-stream solute concentration/signal and discharge. By studying the relationship between DOM and stream discharge, we refine our understanding of the environmental and hydrological factors that influence the quantity and quality of stream DOM. The main objective of this study was to track hysteretic changes in riverine DOM molecular composition during storm events. Samples were collected from nested sites within the Passumpsic River catchment (Vermont, USA), a tributary of the Connecticut River. High-resolution monitoring of fluorescent DOM (via in situ sensors) and automated collection of discrete samples captured short-term, hydrologically driven variations in DOM concentration and composition. Ultrahigh-resolution mass spectrometry revealed an enrichment in aliphatic compounds at storm onset, while aromatic and polyphenolic compounds were more enriched at peak discharge. Molecular hysteresis patterns were similar across stream orders, indicating that fresh, terrigenous DOM is quickly shunted downstream, through the river network, during pulses of high discharge.

Plain Language Summary During storm events, rainfall-runoff processes mobilize large amounts of dissolved organic matter from the land and through river networks. The relationship between stream discharge and dissolved organic matter quantity and composition can vary over the course of a storm event; this variation is termed hysteresis. We examined hysteresis in a forested New England watershed (Vermont, USA) to better understand the location and timing of dissolved organic matter reactivity in river systems. In-stream sensors captured high-frequency, storm-driven changes in dissolved organic matter quantity. Discrete water samples were collected across the storm event for molecular analysis of dissolved organic matter. Molecular analyses revealed differences in dissolved organic matter composition between storm onset and peak discharge. Storm events shunt molecularly diverse organic material further downstream, potentially shifting reactivity hotspots from upper to lower reaches of the watershed.

### 1. Introduction

Rainfall-runoff processes have emerged as key controllers of the quantity and quality of terrestrial dissolved organic matter (DOM) exported from the landscape to inland waters. Hydrological events result in increased river discharge and a concomitant input of large amounts of dissolved organic carbon (DOC) into fluvial networks (Buffam et al., 2001; Dhillon & Inamdar, 2014; Inamdar et al., 2006; Yoon & Raymond, 2012). In New England (USA) forested watersheds, it is estimated that ~60% of annual DOC export occurs during these events (Raymond & Saiers, 2010), spotlighting the importance of event-driven hydrology on DOM flux and reactivity. Observed relationships between DOC and discharge led to the development of the pulse-shunt concept, a theoretical framework for conceptualizing and predicting the impacts of short-term hydrological events on the amount, composition, reactivity, and timing of DOM mobilized through river networks

1

©2019. American Geophysical Union. All Rights Reserved.



(Raymond et al., 2016). The pulse-shunt concept suggests that during periods of high discharge, a large amount of terrestrial DOM is mobilized to rivers (pulse). During these pulse events, rivers transition from active to passive pipes and transport labile, terrestrial DOM further downstream (shunt) than under baseflow conditions. During storms, this event-driven pulse-shunt is proposed to relocate biogeochemical hotspots for DOM processing from the upper to the lower reaches of the watershed (Raymond et al., 2016). To assess how the event-driven export of DOM impacts ecosystem function and carbon cycling a more comprehensive understanding of hydrological controls on the quality and quantity of DOM within rivers is needed.

Hysteresis is defined as the variation in in-stream solute concentration/signal with stream discharge. The analysis of hysteretic patterns illuminates the interplay between watershed hydrology and the quantity and quality of DOM mobilized during storm events (Butturini et al., 2008; Evans & Davies, 1998; House & Warwick, 1998; Lloyd et al., 2016; Vaughan et al., 2017). The slope, rotational direction (clockwise or counterclockwise), and size of hysteresis loops reflect the source, timing, and relative contributions of terrestrial DOM to rivers (Butturini et al., 2006, 2008). For example, elevated DOC concentrations on the falling limb of the discharge hydrograph result in a counterclockwise hysteresis loop, indicating that DOC sources are distal or are transported to the stream via slow-flow pathways (Pellerin et al., 2012). Spectrophotometric techniques (absorbance and fluorescence) have emerged as an efficient means of tracking event-driven changes in DOM quality, revealing higher degrees of aromaticity and humic-like content for DOM exported at high discharge (Eckard et al., 2017; Hood et al., 2006; Inamdar et al., 2011; Vidon et al., 2008). Despite the convenience and utility of these methods, absorbance and fluorescence only represent the chromophoric portion of the DOM pool and lack the molecular-level information that could further advance our biogeochemical understanding of event-mobilized DOM.

Due to its high mass accuracy, Fourier transform ion cyclotron resolution mass spectrometry (FT-ICRMS) can resolve complex DOM mixtures, allowing for the assignment of molecular formulas to individual mass spectral peaks (Dittmar & Koch, 2006; Kujawinski et al., 2002; Sleighter & Hatcher, 2007). FT-ICRMS data yield unique molecular formula fingerprints for individual DOM samples. Each assigned formula represents many possible structural isomers; therefore, a high degree of structural diversity can be contained within the molecular formulas assigned to mass spectral peaks (Zark et al., 2017). While individual formulas cannot be inherently linked to specific molecular structures, their elemental composition is used to categorize formulas into different compound classes (Šantl-Temkiv et al., 2013; Stubbins et al., 2010), which summarizes the chemical character of DOM. Although many molecular formulas are common to DOM from diverse aquatic systems (Lechtenfeld et al., 2014; Wagner et al., 2015), FT-ICRMS has revealed DOM chemistry to vary with watershed climate, land cover, and size (Jaffé et al., 2012; Kim et al., 2006; Mosher et al., 2015). For example, molecular formulas containing nitrogen, sulfur, and phosphorus are enriched in riverine DOM from anthropogenically impacted watersheds (Wagner, Riedel, et al., 2015). The molecular composition of DOM controls its reactivity in aquatic systems (Spencer et al., 2015; Stubbins et al., 2010). In the current study, we used FT-ICRMS to track short-term changes in DOM molecular composition during a storm event (molecular hysteresis) within a forested New England watershed. Samples were collected across the hydrograph at four sites during a November 2016 storm event. Ultrahigh-resolution mass spectral analyses revealed enrichments in aliphatic molecular formulas during storm onset and enrichments in aromatic molecular formulas during and after peak discharge. Biogeochemical implications for the rapid mobilization of potentially reactive DOM during storm events are discussed.

### 2. Methods

### 2.1. Site Description

Samples and data were collected from nested sites within the Passumpsic River watershed, a tributary of the Connecticut River in northern Vermont (USA; Figure 1). W-9 is a first-order stream (drainage area = 0.41 km²) with a completely forested watershed. Pope Brook is a third-order stream (drainage area = 8.37 km²) within a primarily forested watershed (81% of basin area) with some areas of agriculture (14%). Sleepers River is a fourth-order stream (drainage area = 111.3 km²) within a predominantly forested watershed (75%) with areas of agriculture (14%). Passumpsic River is a sixth-order stream (drainage area = 1,124 km²) within a primarily forested watershed (77%), with some agriculture (8%) and wetland cover (4%). Pope, Sleepers, and Passumpsic also have some developed area within their catchment (3–6%).

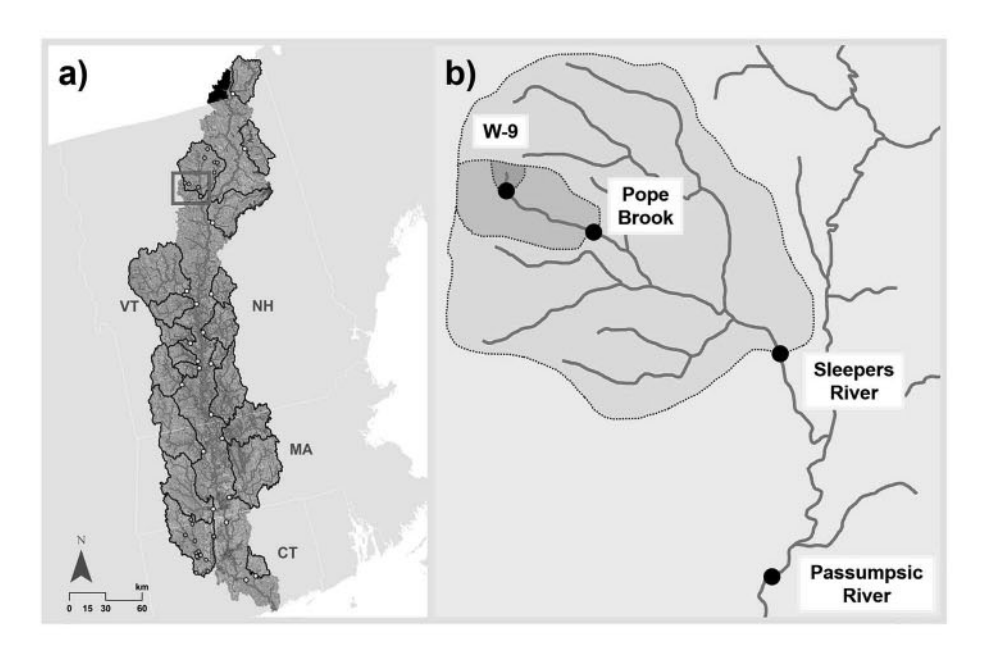


Figure 1. (a) Map of the greater Connecticut River watershed. Samples were collected from the Passumpsic River and its tributaries, located within the red box. (b) Zoomed in map showing the four nested sampling sites. The black circles indicate stream sampling locations. The black dotted lines contain drainage areas for W-9, Pope Brook, and Sleepers River.

The Sleepers River location is the outlet of the Sleepers River Research Watershed, a site of long-term hydrological and biogeochemical research (Shanley et al., 2015). Discharge records were obtained from U.S. Geological Survey (USGS) gaging stations for W-9 (Pope Brook Tributary; USGS station no. 01135100), Pope (Pope Brook; USGS station no. 01135150), Sleepers (Sleepers River; USGS station no. 01135300), and Passumpsic (Passumpsic River; USGS station no. 01135500).

### 2.2. In Situ Fluorescent DOM

Fluorescent dissolved organic matter (FDOM), temperature (°C), and turbidity (formazin normalized units) were measured in situ at 15-min intervals using Eureka Manta 2 water quality sondes (Eureka Water Probes, Austin, TX, USA). Sondes were deployed at the W-9, Pope, Sleepers, and Passumpsic sampling sites from May 2015 through August 2017, capturing a storm event from 3 to 4 November 2016. Sondes were co-located with USGS gages where possible. FDOM readings were collected using a Turner Designs (San Jose, CA) submersible fluorescent sensor using an excitation window at 325  $\pm$  120 nm and an emission window at 470  $\pm$  60 nm. Sensors were calibrated following manufacturer specifications and USGS protocols (Radtke et al., 2005). FDOM sensors were calibrated using a six-point quinine sulfate solution calibration curve with a maximum concentration of 1000  $\mu$ M. Turbidity was calibrated to formazin normalized units using formazin turbidity standard (Ricca Chemical Company; Arlington, TX). Once offloaded, all sonde data were checked and measurements impacted by bio-fouling or instrument malfunction were removed from the final data set.

FDOM measurements were corrected for impacts of stream water temperature, turbidity, and light absorbance on DOM fluorescence following standard methods (Downing et al., 2012) with two modifications. First, rather than use a standard temperature-FDOM relationship, we assessed temperature dependence of DOM fluorescence at each site (equation S1). Second, we developed an empirical relationship between turbidity and fluorescence attenuation using sediment collected from Bunnell Brook (USGS station no. 01188000) and Hubbard River (USGS station no. 01187300) for turbidity correction (equation (S2)). The temperature- and turbidity-corrected FDOM was then corrected for light absorbance for each site (equation (S3)). FDOM corrections are described in detail in the supporting information and reported here in quinine sulfate equivalents (QSEs).

### 2.3. Sample Collection and DOC Analysis

Water samples were collected by automated samplers (ISCO Avalanche) triggered by threshold changes in stream stage. Thresholds were optimized at each site to obtain a comprehensive set of samples over the



rising limb, peak, and falling limb of the storm hydrograph. Since W-9 is a first order stream, discharge at this site peaks and recedes rapidly in response to a rain event. Due to the flashy hydrology and longer temporal spacing of sampling ( $\sim$ 1.5 hr) at W-9, the autosampler captured fewer water samples during the event at W-9 (n=3) than at Pope (n=14), Sleepers (n=14), and Passumpsic (n=13). Samples were brought in from the field within 24 hr and transported to the laboratory where they were filtered ( $0.2 \mu m$ ), acidified (to pH 2 using hydrochloric acid), and refrigerated until further analysis. DOC was measured as nonpurgable organic carbon using a Shimadzu total organic carbon analyzer (Stubbins & Dittmar, 2012) within 10 days of sample collection. A calibration curve was made by analyzing dilutions of a potassium hydrogen phthalate stock solution and then used to quantify DOC in discrete samples.

### 2.4. Solid Phase Extraction of DOM

Filtered samples for FT-ICRMS analysis were frozen until solid phase extraction (SPE) by passing the acidified sample through a Varian Bond Elut PPL cartridge (100 mg) as described by Dittmar et al. (2008). Water was acidified to pH 2 using concentrated HCl. The SPE sorbent was first conditioned with methanol, then equilibrated with pH 2 Milli-Q water prior to DOM extraction. The acidified sample was then passed through the cartridge via gravity. The volume of sample passed through each SPE cartridge was carbon-normalized. For each sample, the target amount of DOC applied to the sorbent was ~170  $\mu$ g-C. This equated to a target DOC recovery of 100  $\mu$ g-C, since SPE PPL DOC recovery for riverine samples is typically ~60% (Dittmar et al., 2008). After extraction, the sorbent was rinsed with pH 2 Milli-Q water for the removal of excess salts prior to drying under a stream of carbon-free air. The DOM was then eluted from the sorbent with high-purity methanol into a precombusted glass vial and stored in the dark at -20 °C until FT-ICR mass spectral analysis.

### 2.5. Fourier Transform Ion Cyclotron Resonance Mass Spectrometry

To obtain consistent FT-ICR mass spectra, all samples were prepared and analyzed under the same conditions. The DOM-containing methanol extracts were each mixed with Milli-Q water (1:1 v/v) to yield a final DOC concentration of 5 mg-C/L. The samples were then continuously infused into the electrospray ionization source of a Bruker Solarix 15 T FT-ICRMS instrument (University of Oldenburg, Germany) at a flow rate of  $120 \,\mu$ l/hr in negative ion mode (175 scans per sample, ion accumulation time = 0.200 s). The raw mass spectra were calibrated using a reference mass list to achieve mass accuracies with an error less than 0.1 ppm. Mass spectra were filtered to exclude peaks that were found to be present in less than three samples across the data set and noise peaks, as defined by the method detection limit (Riedel & Dittmar, 2014). The method detection limit is a noise correction approach described in detail by Riedel and Dittmar (2014), which assesses noise from sample mass spectra in mass ranges where peaks for singly charged organic molecules cannot occur (mass defects between 0.3 and 0.9 Da). Peak detection limits were standardized among samples by adjusting the dynamic range of mass spectral peak abundances of each sample to that with the lowest dynamic range based upon Stubbins et al. (2014). For each sample, the dynamic range was calculated as the mean peak abundance of the 500 highest abundance mass peaks divided by the mean abundance of the 10 lowest abundance mass peaks. The standardized detection limit (SDL) was then set for each sample by dividing the mean peak abundance of the 500 highest abundance mass peaks by the lowest calculated dynamic range value within the sample set. For each sample, mass peaks with abundances lower than the SDL were removed. Equations used for calculating the dynamic range and SDL are included in the supporting information.

Elemental formulas containing C, H, O, N, S, and/or P were assigned to mass spectral peaks according to published rules (Koch et al., 2007; Singer et al., 2012; Stubbins et al., 2010). Specific methods used for formula assignment and screening in the current study are detailed in the supporting information. Assigned formulas were categorized by compound class according to elemental stoichiometries (Šantl-Temkiv et al., 2013). The modified aromaticity index (AI<sub>mod</sub>; Koch & Dittmar, 2006, 2016) was used to identity formulas that were aromatic (polyphenols;  $0.5 \le AI_{mod} < 0.67$ ) and condensed aromatic (AI<sub>mod</sub>  $\le 0.67$ ). Formulas were further categorized into highly unsaturated (AI<sub>mod</sub> < 0.5, H/C < 1.5, O/C < 0.9) and unsaturated aliphatic ( $1.5 \le H/C < 2$ , O/C < 0.9, N = 0) compounds. Individual formulas represent multiple isomeric structures. As such, a degree of potential structural diversity is contained within the molecular formulas assigned to mass spectral peaks (Zark et al., 2017). Therefore, the above-described compound classifications only serve as a guide when interpreting mass spectral data and considering the molecular structures present

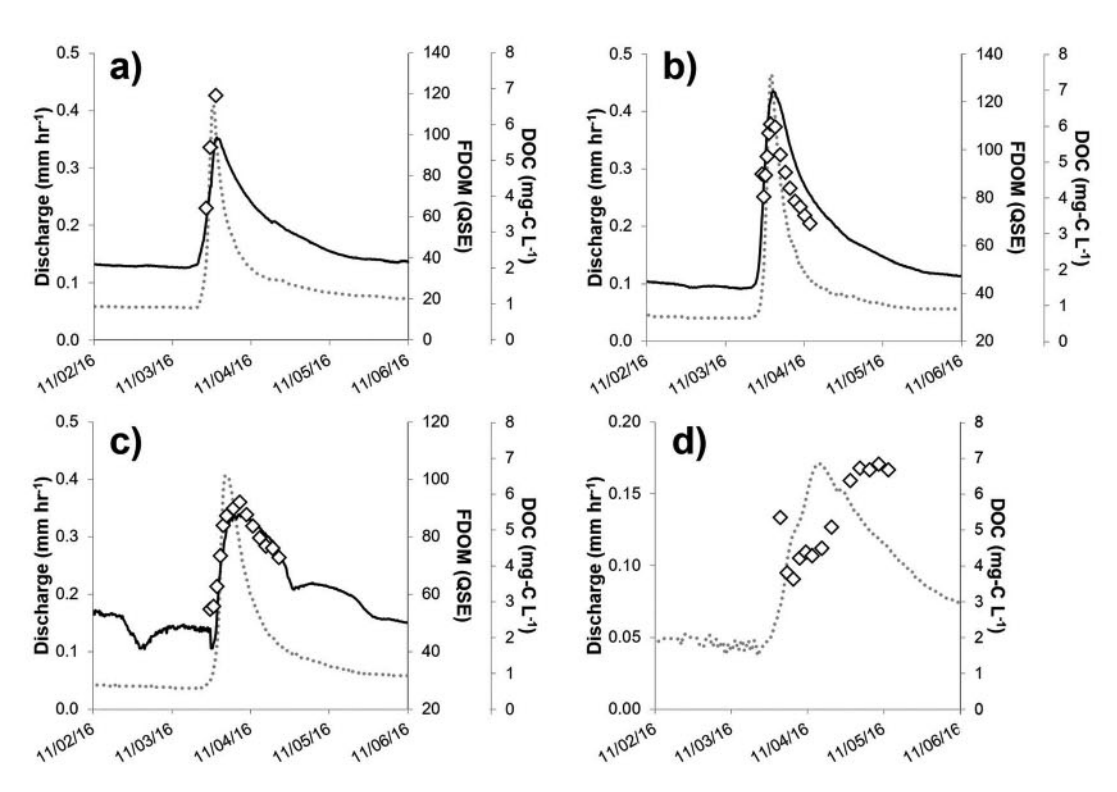


Figure 2. Stream discharge (grey, dotted line), in situ fluorescent dissolved organic matter (FDOM; black, solid line), and dissolved organic carbon (DOC) concentration (white diamonds) during the storm event at (a) W-9, (b) Pope Brook, (c) Sleepers River, and (d) Passumpsic River. In situ FDOM data for Passumpsic were not available for this storm event.

within DOM. Electrospray ionization (in negative ion mode) coupled with FT-ICRMS preferentially ionizes and detects polar, organic compounds, which makes it the analytical method of choice for the molecular characterization of complex DOM mixtures (Kim et al., 2003; Kujawinski, 2002). However, it is well understood that ionization efficiencies are not equal among different molecules and compound classes. Therefore, observed variations in the relative abundance of FT-ICR mass peaks may not accurately reflect actual molecular concentrations or represent the molecular diversity of the entire DOM pool.

### 3. Results

### 3.1. Event-Driven Variations in Discharge

The early November 2016 storm sampled here resulted in an increase in stream discharge by roughly an order of magnitude above baseflow at all nested sites (Figure 2). Prestorm baseflow at W-9 was 0.056 mm/hr and reached a maximum discharge of 0.41 mm/hr at peak flow. At Pope, prestorm baseflow was 0.040 and 0.46 mm/hr at peak discharge. Prestorm baseflow at Sleepers was 0.037 mm/hr and reached a maximum discharge of 0.41 mm/hr at peak flow. At Passumpsic, prestorm baseflow was 0.044 and 0.17 mm/hr at peak discharge. Discharge for each sampling event is listed in Table 1. Peak discharge at W-9, Pope, Sleepers, and Passumpsic was higher than the average storm event that typically occurs in this region (based upon the average peak discharge within the last 2 years). The time lag of peak discharge from W-9 at Pope, Sleepers, and Passumpsic was 1.5, 4.75, and 15 hr, respectively.

### 3.2. Event-Driven Variations in In Situ FDOM

In situ sondes at W-9, Pope, and Sleepers simultaneously captured in-stream FDOM throughout the storm event. The sonde at Passumpsic was not functioning during the storm; therefore, continuous FDOM data for this site are not available. At W-9, prestorm baseflow FDOM was 35 QSE, increasing to 91 QSE at peak discharge (Figure 2a). At Pope, FDOM was 43 QSE during prestorm baseflow and increased to 120 QSE at peak discharge (Figure 2b). At Sleepers, prestorm baseflow FDOM averaged 45 QSE, increasing to 85 QSE at peak discharge (Figure 2c). At W-9, Pope, and Sleepers, peak FDOM signal occurred after peak discharge. FDOM values for individual samples are listed in Table 1.



Table 1

Data and Sample Information for Samples Collected During the November 2016 Storm Event

| Site       | Date            | Time  | Discharge (mm/hr) | DOC (mg-C/L) | FDOM (QSE) | Mass (Da) | H/C  | O/C  | AI <sub>mod</sub> |
|------------|-----------------|-------|-------------------|--------------|------------|-----------|------|------|-------------------|
| W-9        | 3 November 2016 | 10:13 | 0.13              | 3.68         | 58         | 329       | 0.88 | 0.32 | 0.31              |
| W-9        | 3 November 2016 | 11:23 | 0.33              | 5.37         | 74         | 322       | 0.84 | 0.32 | 0.33              |
| W-9        | 3 November 2016 | 13:08 | 0.36              | 6.81         | 98         | 322       | 0.84 | 0.32 | 0.33              |
| Pope       | 3 November 2016 | 11:15 | 0.090             | 4.66         | 71         | 328       | 1.00 | 0.31 | 0.26              |
| Pope       | 3 November 2016 | 11:45 | 0.12              | 4.02         | 85         | 332       | 0.95 | 0.31 | 0.29              |
| Pope       | 3 November 2016 | 12:15 | 0.19              | 4.62         | 96         | 335       | 0.91 | 0.32 | 0.30              |
| Pope       | 3 November 2016 | 12:45 | 0.28              | 5.15         | 108        | 326       | 0.90 | 0.32 | 0.31              |
| Pope       | 3 November 2016 | 13:15 | 0.39              | 5.81         | 114        | 327       | 0.91 | 0.31 | 0.30              |
| Pope       | 3 November 2016 | 13:45 | 0.46              | 6.06         | 120        | 329       | 0.90 | 0.31 | 0.30              |
| Pope       | 3 November 2016 | 15:18 | 0.39              | 5.97         | 124        | 318       | 0.87 | 0.30 | 0.31              |
| Pope       | 3 November 2016 | 16:48 | 0.29              | 5.20         | 119        | 324       | 0.90 | 0.31 | 0.30              |
| Pope       | 3 November 2016 | 18:18 | 0.22              | 4.71         | 110        | 337       | 0.91 | 0.31 | 0.30              |
| Pope       | 3 November 2016 | 19:48 | 0.18              | 4.27         | 102        | 330       | 0.90 | 0.31 | 0.30              |
| Pope       | 3 November 2016 | 21:18 | 0.16              | 3.90         | 95         | 330       | 0.89 | 0.31 | 0.30              |
| Pope       | 3 November 2016 | 22:48 | 0.13              | 3.73         | 89         | 331       | 0.90 | 0.32 | 0.30              |
| Pope       | 4 November 2016 | 00:18 | 0.12              | 3.50         | 85         | 338       | 0.92 | 0.31 | 0.29              |
| Pope       | 4 November 2016 | 01:48 | 0.11              | 3.27         | 81         | 339       | 0.92 | 0.31 | 0.29              |
| Sleepers   | 3 November 2016 | 11:39 | 0.048             | 2.79         | 48         | 329       | 0.95 | 0.30 | 0.29              |
| Sleepers   | 3 November 2016 | 12:39 | 0.068             | 2.87         | 43         | 322       | 0.94 | 0.30 | 0.29              |
| Sleepers   | 3 November 2016 | 13:39 | 0.11              | 3.42         | 51         | 327       | 0.94 | 0.31 | 0.29              |
| Sleepers   | 3 November 2016 | 14:39 | 0.22              | 4.28         | 67         | 325       | 0.92 | 0.30 | 0.30              |
| Sleepers   | 3 November 2016 | 15:39 | 0.38              | 5.11         | 75         | 331       | 0.93 | 0.32 | 0.29              |
| Sleepers   | 3 November 2016 | 16:39 | 0.41              | 5.38         | 83         | 327       | 0.91 | 0.31 | 0.30              |
| Sleepers   | 3 November 2016 | 18:41 | 0.36              | 5.59         | 87         | 325       | 0.91 | 0.31 | 0.30              |
| Sleepers   | 3 November 2016 | 20:41 | 0.29              | 5.77         | 87         | 336       | 0.90 | 0.31 | 0.30              |
| Sleepers   | 3 November 2016 | 22:41 | 0.23              | 5.41         | 86         | 331       | 0.89 | 0.30 | 0.30              |
| Sleepers   | 4 November 2016 | 00:41 | 0.19              | 5.10         | 85         | 325       | 0.90 | 0.31 | 0.31              |
| Sleepers   | 4 November 2016 | 02:41 | 0.16              | 4.76         | 83         | 338       | 0.92 | 0.33 | 0.30              |
| Sleepers   | 4 November 2016 | 04:41 | 0.14              | 4.54         | 80         | 333       | 0.90 | 0.31 | 0.30              |
| Sleepers   | 4 November 2016 | 06:41 | 0.12              | 4.49         | 79         | 336       | 0.89 | 0.31 | 0.31              |
| Sleepers   | 4 November 2016 | 08:41 | 0.11              | 4.24         | 75         | 338       | 0.90 | 0.31 | 0.30              |
| Passumpsic | 3 November 2016 | 15:27 | 0.073             | 5.34         | N/A        | 325       | 0.99 | 0.32 | 0.27              |
| Passumpsic | 3 November 2016 | 17:27 | 0.10              | 3.80         | N/A        | 326       | 0.91 | 0.31 | 0.30              |
| Passumpsic | 3 November 2016 | 19:27 | 0.12              | 3.62         | N/A        | 330       | 0.93 | 0.31 | 0.29              |
| Passumpsic | 3 November 2016 | 21:27 | 0.13              | 4.21         | N/A        | 330       | 0.93 | 0.31 | 0.30              |
| Passumpsic | 3 November 2016 | 23:27 | 0.15              | 4.37         | N/A        | 330       | 0.92 | 0.32 | 0.30              |
| Passumpsic | 4 November 2016 | 01:27 | 0.16              | 4.28         | N/A        | 331       | 0.92 | 0.32 | 0.30              |
| Passumpsic | 4 November 2016 | 04:31 | 0.17              | 4.47         | N/A        | 332       | 0.90 | 0.31 | 0.30              |
| Passumpsic | 4 November 2016 | 07:31 | 0.16              | 5.07         | N/A        | 331       | 0.90 | 0.32 | 0.30              |
| Passumpsic | 4 November 2016 | 13:31 | 0.14              | 6.36         | N/A        | 327       | 0.89 | 0.32 | 0.30              |
| Passumpsic | 4 November 2016 | 16:31 | 0.13              | 6.71         | N/A        | 328       | 0.88 | 0.32 | 0.31              |
| Passumpsic | 4 November 2016 | 19:31 | 0.12              | 6.67         | N/A        | 331       | 0.89 | 0.32 | 0.31              |
| Passumpsic | 4 November 2016 | 22:31 | 0.12              | 6.82         | N/A        | 329       | 0.89 | 0.32 | 0.31              |
| Passumpsic | 5 November 2016 | 01:31 | 0.11              | 6.66         | N/A        | 337       | 0.88 | 0.32 | 0.31              |

Note. Includes date and time of sample collected, stream discharge, dissolved organic carbon (DOC) concentration, and in situ fluorescent dissolved organic matter (FDOM) signal. Abundance-weighted average values for molecular formula mass (Da), H/C ratio, O/C ratio, and the aromaticity index ( $AI_{mod}$ ) are also listed. QSE, quinine sulfate equivalent.

### 3.3. Event-Driven Variations in DOC Concentration

At Pope, Sleepers, and Passumpsic, 13 to 14 individual samples were collected across the hydrograph to capture changes in DOC along the rising and falling limbs (Figure 2 and Table 1). Since W-9 is a first-order stream with flashy hydrology, only three samples were collected during this storm event (two samples on the rising limb and one sample just after peak discharge; Figure 2a and Table 1). At W-9, DOC concentrations ranged from 3.68 to 6.81 mg-C/L. The initial storm sample at Pope had a DOC concentration of 4.66 mg-C/L, but DOC then dropped to 4.02 mg-C/L before DOC concentrations increased again (Figure 2a and Table 1). Peak DOC concentration at Pope was 6.06 mg-C/L, which closely coincided with peak discharge (Figure 2b). At Sleepers, DOC concentrations ranged from 2.79 mg-C/L at storm onset to 5.77 mg-C/L just after peak discharge (Figure 2c and Table 1). At Passumpsic, DOC concentration was

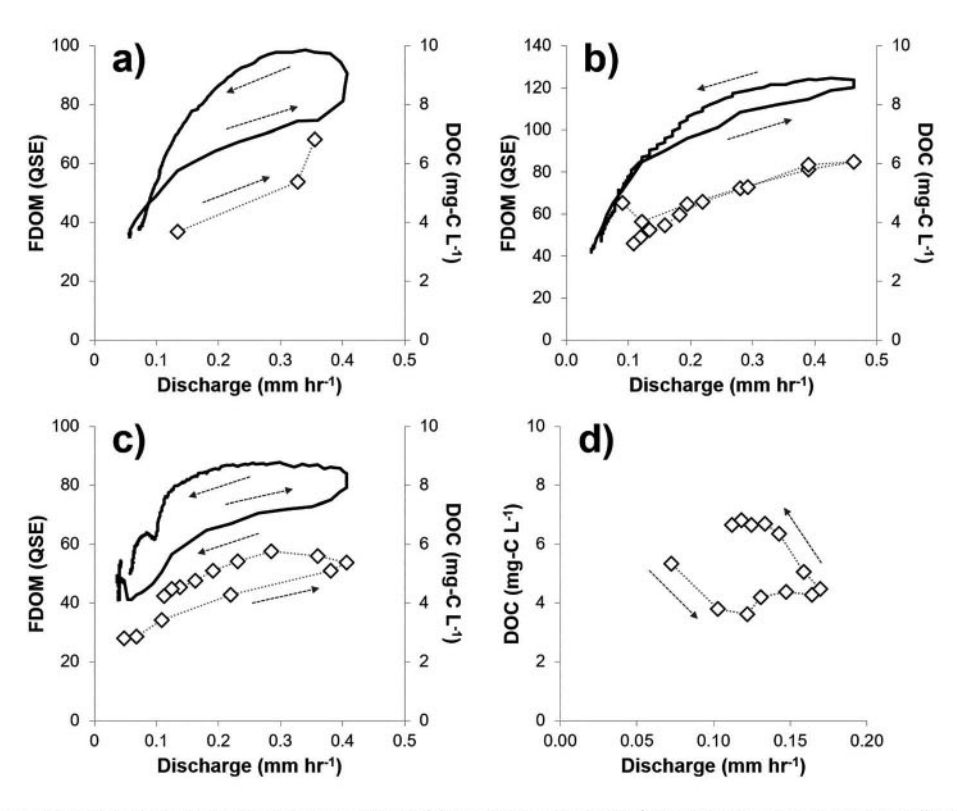


Figure 3. In situ fluorescent dissolved organic matter (FDOM; black, solid line) and dissolved organic carbon (DOC) concentration (white diamonds) versus discharge at (a) W-9, (b) Pope Brook, (c) Sleepers River, and (d) Passumpsic River. The dashed arrows indicate temporal direction from storm onset to falling limb.

5.34 mg-C/L at event onset, decreased to 3 to 4 mg-C/L during the rising limb and at peak discharge, and then peaked at 6.82 mg-C/L roughly 18 hr after peak discharge (Figure 2d and Table 1).

### 3.4. Hysteresis in DOC Concentration and In Situ FDOM

While the number of discrete samples collected at W-9 was small (n = 3), continuous FDOM data showed a clear positive correlation with discharge and a counterclockwise hysteresis (Figure 3a), which suggested that a similar hysteretic trend would be observed for DOC if discrete samples were collected at higher frequency across the hydrograph. At Pope, DOC was positively related to discharge with no apparent hysteresis (i.e., the relationship between DOC and discharge was the same on the rising and falling limbs of the hydrograph; Figure 3b), whereas the FDOM data were positively related to discharge, with a counterclockwise hysteresis (Figure 3b). At Sleepers, DOC was positively related to discharge and exhibited a concave, counterclockwise hysteresis loop and FDOM was positively related to discharge, with a counterclockwise hysteresis (Figure 3c). At Passumpsic, where FDOM data were lacking, the slope of the relationship between DOC and discharge was flat (near zero) and had a counterclockwise, convex hysteresis loop (Figure 3d).

### 3.5. Comparison of DOM Molecular Composition Across Sites

Raw mass spectra showed peak distributions consistent with those observed for other river DOM samples (Figure 4; Wagner, Riedel, et al., 2015). In total, 6,148 unique molecular formulas were assigned to FT-ICRMS peaks across all samples (n = 44). The number of formulas assigned per DOM sample ranged from 4,210 to 4,752. The mean number of formulas assigned to samples collected from W-9 (n = 3), Pope (n = 14), Sleepers (n = 14), and Passumpsic (n = 13) did not vary significantly (mean  $\pm$  SD): 4,568  $\pm$  179, 4,484  $\pm$  134, 4,591  $\pm$  105, and 4,574  $\pm$  136, respectively (t test; p > 0.05; Table 2). Assigned molecular formulas spanned a mass range of 95 to 775 Da. Most of the molecular formulas contained only C, H, and O (n = 3283). The remaining formulas (n = 2865) contained N, S, P, or a combination thereof. Mean abundance-weighted average values for molecular mass at Pope, Sleepers, and Passumpsic were 330 Da with standard deviations of 6, 5, and 3 Da, respectively. Mean abundance-weighted average values for H/C at Pope, Sleepers, and Passumpsic were 0.91 with standard deviations of 0.03, 0.02, and 0.03, respectively. Mean abundance-

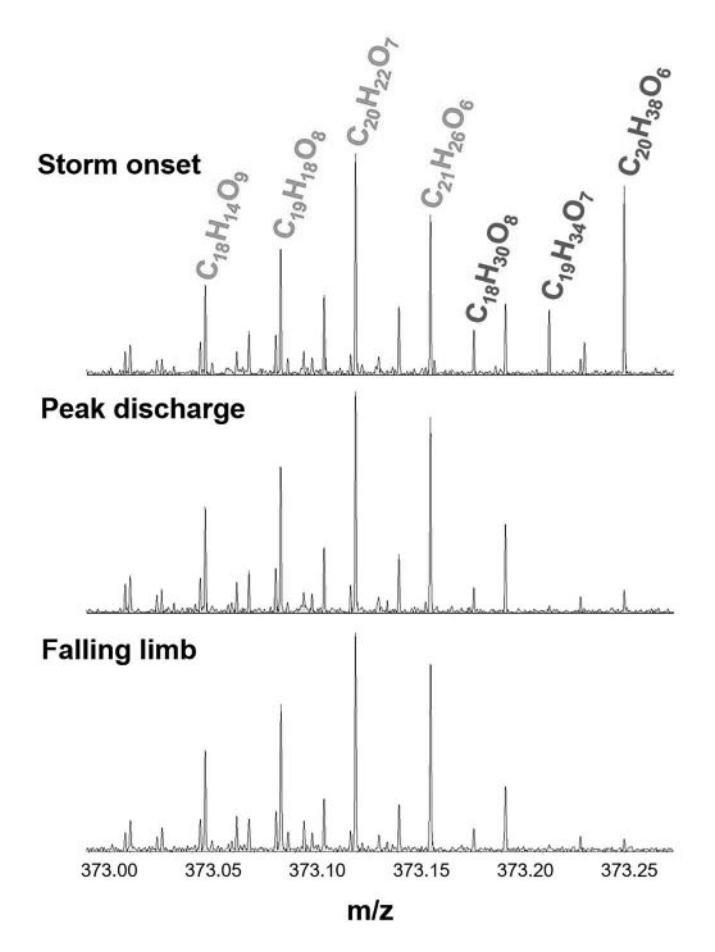


Figure 4. Exemplary raw mass spectra featuring peaks at 373 m/z for samples collected at Pope Brook during storm onset (3 November 2016 11:15 a.m.), peak discharge (3 November 2016 1:15 p.m.), and from the falling limb of the hydrograph (4 November 2016 12:18 a.m.). Molecular formulas in purple are assigned to mass spectral peaks, which were enriched at storm onset. Molecular formulas in green are assigned to mass spectral peaks, which are persistent and/or enriched at peak discharge and along the falling limb of the hydrograph.

weighted average values for  $AI_{mod}$  at Pope, Sleepers, and Passumpsic were  $0.30\pm0.01$ . Samples collected at W-9 exhibited, on average, lower molecular mass (324  $\pm$  4 Da), lower H/C (0.85  $\pm$  0.02), and higher  $AI_{mod}$  (0.32  $\pm$  0.01) than those collected at higher stream orders. There was no apparent trend in mean abundance-weighted average O/C values across the stream orders (values ranged from 0.31 to 0.32). The average proportion of molecular formulas identified as condensed aromatics (13%), polyphenols (17%), highly unsaturated compounds (54%), and unsaturated aliphatics (12%) did not significantly vary among stream orders (p > 0.05; Table 2). Abundance-weighted average values of molecular mass, H/C, O/C, and  $AI_{mod}$  for individual samples are listed in Table 1. Mean and standard deviation values for the number of assigned formulas and the proportion of formulas in each molecular category are listed in Table 2.

### 3.6. Event-Driven Variations in DOM Molecular Composition

While average molecular characteristics across the nested sites were relatively consistent, the molecular composition of DOM varied at each site across the hydrograph. Figure 4 compares raw mass spectra for Pope Brook, collected at storm onset, peak discharge, and along the falling limb, at 373 m/z. Peaks at higher mass defects (0.18-0.26 Da) were found to be more abundant (i.e., have a higher relative peak intensity) at storm onset (Figure 4). Formulas assigned to peaks at higher mass defects have high H/C ratios (>1.5) compared to formulas assigned to peaks at lower mass defects. Many of these high mass defect peaks decreased in abundance or fell below the limit of detection in peak discharge and falling limb samples (Figure 4). The preliminary comparison of raw DOM mass spectra was the first indication of varied DOM molecular composition during the storm event. Plotting relative peak abundance against discharge revealed hysteresis of individual molecular formulas (Figures 5 and 6). Some formulas were more enriched on the rising limb and more depleted on the falling limb, resulting in clockwise molecular hysteresis (e.g., C<sub>19</sub>H<sub>30</sub>O<sub>4</sub> at Pope, Sleepers, and Passumpsic; Figures 5b-5d). Other formulas were more depleted on the rising limb and became more enriched on the falling limb, resulting in counterclockwise molecular hysteresis (e.g., C15H8O9 at Sleepers and Passumpsic; Figures 6c and 6d). The

hysteresis of individual molecular formulas was not always similar across stream orders. For example, although the molecular formula  $C_{15}H_8O_9$  was more enriched at peak discharge relative to storm onset, the relationship between relative peak abundance and discharge did not exhibit the clear counterclockwise shape observed at Sleepers and Passumpsic (Figures 6b–6d). The hysteresis of individual molecular formulas contributed to observed shifts in bulk DOM composition during the storm event. At W-9, Pope, Sleepers, and Passumpsic, the abundance-weighted average H/C ratio decreased from 0.88 to 0.84, 1.00 to 0.90, 0.95 to 0.91, and 0.99 to 0.90, respectively, between storm onset and peak discharge (Table 1 and Figure 7). After peak discharge, on the falling limb of the hydrograph, H/C ratios remained low across all sites (Table 1 and Figure 7).

Table 2

Mean (±1 SD) Values for the Total Number of Formulas Assigned and Proportion of Molecular Formulas Categorized to Each Compound Class for Samples Collected at Each Nested Site

| Site       | No. assigned formulas | Condensed aromatics (%) | Polyphenols (%)  | Highly unsaturated (%) | Unsaturated aliphatics (%) |  |
|------------|-----------------------|-------------------------|------------------|------------------------|----------------------------|--|
| W-9        | 4,568 ± 179           | 13.7 ± 0.5%             | 17.2 ± 0.5%      | 54.1 ± 1.0%            | 12.3 ± 1.1%                |  |
| Pope       | $4,484 \pm 134$       | $13.4 \pm 0.5\%$        | $17.3 \pm 0.4\%$ | $54.2 \pm 1.2\%$       | $12.6 \pm 1.2\%$           |  |
| Sleepers   | $4,591 \pm 105$       | $13.1 \pm 0.4\%$        | $17.2 \pm 0.3\%$ | $54.9 \pm 1.0\%$       | $12.1 \pm 1.0\%$           |  |
| Passumpsic | $4,574 \pm 136$       | $13.3 \pm 0.4\%$        | $17.3 \pm 0.4\%$ | $54.3 \pm 0.5\%$       | $12.4 \pm 0.7\%$           |  |

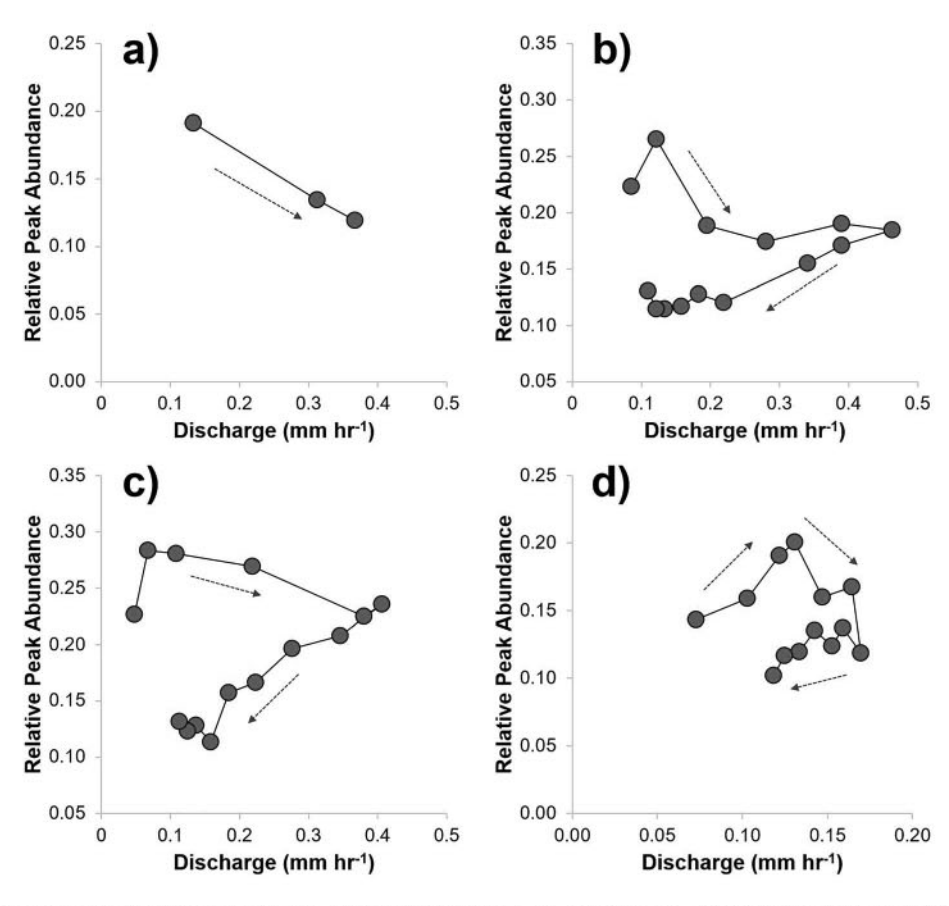


Figure 5. Single peak hysteresis for the molecular formula  $C_{19}H_{30}O_4$  (exact mass = 322.214410 Da) at (a) W-9, (b) Pope Brook, (c) Sleepers River, and (d) Passumpsic River.

To compare molecular hysteretic trends across sites, mass spectral data were split into subsets based upon sampling location (W-9, n = 3; Pope, n = 14; Sleepers, n = 14; and Passumpsic, n = 13) for further analysis. The abundance of mass spectral peaks were normalized across each subset so abundance values for an individual mass peak ranged from 0 to 1 (where 0 and 1 represented the points at which a particular mass peak had the lowest and highest abundance, respectively, across the hydrograph). The normalization of mass spectral peaks within each subset of samples allowed for the direct comparison of hysteretic behavior of thousands of individual assigned formulas at each sampling site. The onset-peak index (which ranges from -1 to +1) was then calculated by subtracting the normalized abundance of a peak in the DOM sample collected at storm onset from the normalized peak abundance in the DOM sample collected at peak discharge. Methodological details and example of how onset-peak indices were calculated is described in the supporting information. An onset-peak index >0 indicated that a molecular formula was more enriched at storm onset than at peak discharge. An onset-peak index <0 indicated that a molecular formula was more enriched at peak discharge than at storm onset. An onset-peak value = 0 indicated that the molecular formula enrichment was the same at storm onset and peak discharge. The formulas identified in storm samples at each site (W-9, Pope, Sleepers, and Passumpsic) are displayed in van Krevelen space, where H/C ratios are plotted against O/C ratios (Figure 8). In Figure 8, each data point represents a single molecular formula and is colored based upon its onset-peak index.

### 4. Discussion

### 4.1. Interpreting DOC and FDOM Hysteresis in a Nested Watershed

DOC concentration and FDOM signal generally increased with increasing discharge across the nested sites. Positive, counterclockwise hysteresis relationships between DOC and discharge are commonly observed for tributaries of the Passumpsic River (Pellerin et al., 2012; Shanley et al., 2015). In our results, except for Pope,

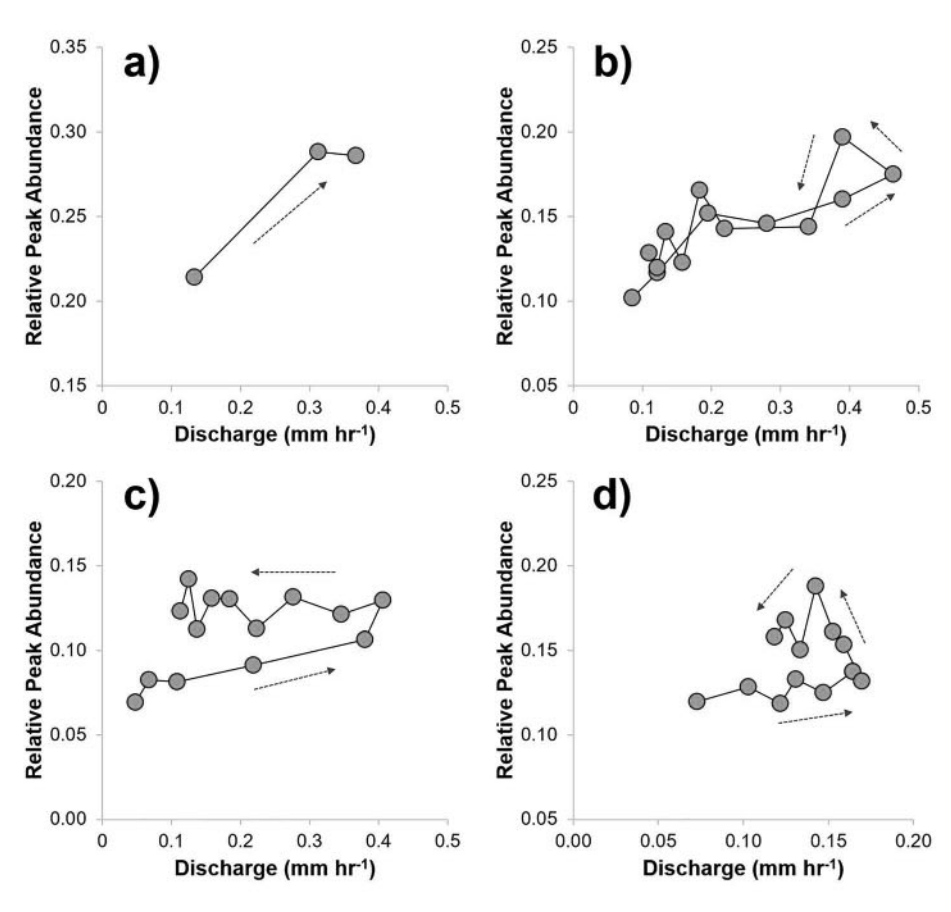


Figure 6. Single-peak hysteresis for the molecular formula  $C_{15}H_8O_9$  (exact mass = 332.016835 Da) at (a) W-9, (b) Pope Brook, (c) Sleepers River, and (d) Passumpsic River.

hysteresis patterns for DOC were also counterclockwise (Figure 3). Although the number of discrete samples collected at W-9 was small (n = 3), DOC was positively related to discharge and we can assume a counterclockwise hysteresis loop based upon the counterclockwise trend in FDOM (Figure 3a). A peak in DOC concentration after peak discharge indicated that water with the highest DOC concentrations arrived latest to the stream. The late arrival of the most DOC-rich waters at W-9, Sleepers, and Passumpsic could be due to DOC-rich waters originating in sites geographically distal from the stream (Pellerin et al., 2012) and/or from DOC-rich waters taking flow paths through soils with slower responses than those of groundwater and surface flow (Evans & Davies, 1998). The closed loop between DOC and discharge indicates two component mixing for in-stream DOM at Pope (Figure 3b), where baseflow water (low DOC, low FDOM) mixes with event water (high DOC, high FDOM). Using classical interpretations, closed loop hysteresis can also indicate that the concentrations of DOC in both surface event water (overland flow, direct precipitation) and soil water were roughly equivalent to one another and greater than DOC concentrations in groundwater (Evans & Davies, 1998). While the hysteresis patterns observed in the current study are consistent with historical data (Shanley et al., 2015), the relationship between DOC, FDOM, and discharge within the Passumpsic River watershed is known to be dynamic throughout the year (Pellerin et al., 2012). Therefore, the current set of data, which focuses upon a single storm event, may not be representative of all hysteresis patterns observed for the Passumpsic River and its tributaries.

### 4.2. Distinct Molecular Signatures at Storm Onset and Peak Discharge

FT-ICRMS data show a depletion in aromatic compounds during storm onset and an enrichment in aromatic compounds during peak discharge (Figure 8). High H/C (>1) molecular formulas were enriched at storm onset (Figure 9a). Formulas prevalent at storm onset were primarily categorized as unsaturated aliphatics and are described as lipid-like, carboxylic-rich alicyclic molecules (Hertkorn et al., 2006) and lignin degradation products. The potential for high structural diversity (isomeric plasticity) prevents the

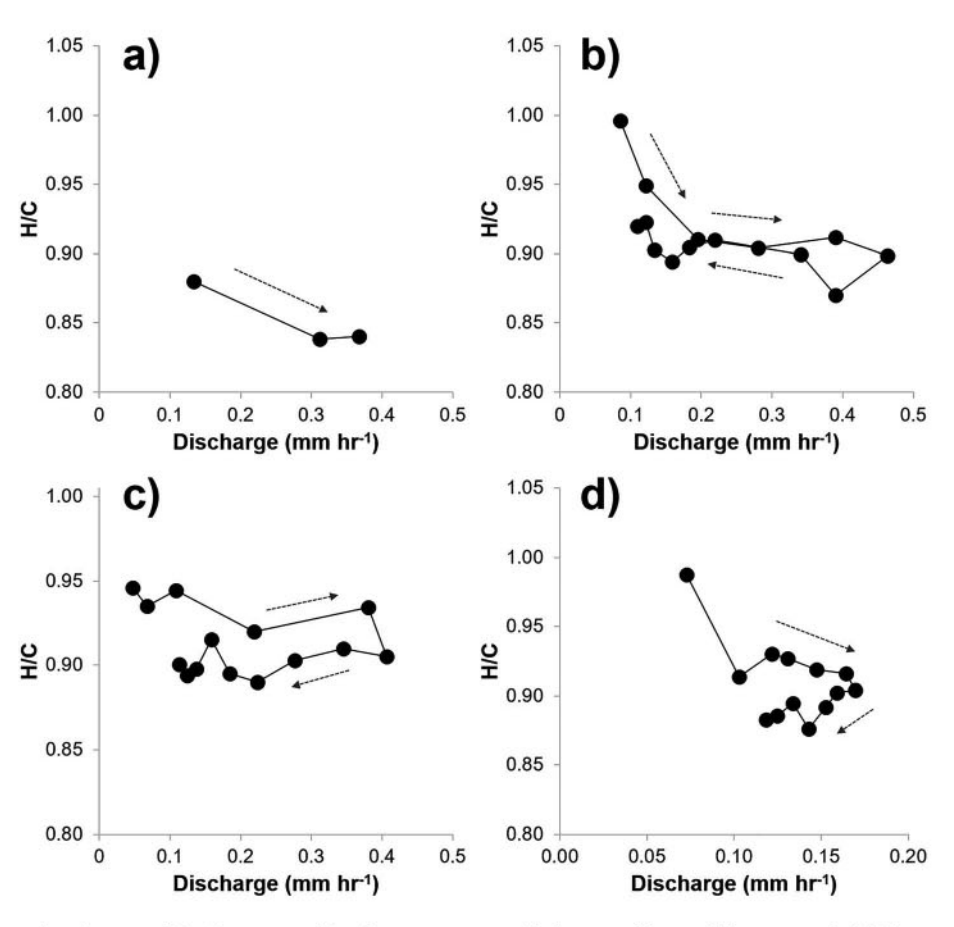


Figure 7. Abundance-weighted average H/C ratios versus stream discharge at (a) W-9, (b) Pope Brook, (c) Sleepers River, and (d) Passumpsic River. The dashed arrows indicate temporal direction from storm onset to falling limb.

assignment of these formulas to more refined molecular categories (Stubbins et al., 2010). Low H/C (<1) molecular formulas were enriched during peak discharge (Figure 9b). Formulas prevalent at peak discharge were primarily categorized as highly unsaturated, polyphenolic (lignin degradation products and tannins), and condensed aromatic (dissolved black carbon) compounds (Figure 9b). The aromatic molecular formula signature of DOM exported at high flow is consistent with previous studies, which show an elevated export of aromatic- and humic-rich DOM (Hood et al., 2006; Inamdar et al., 2011; Vidon et al., 2008), lignin (Eckard et al., 2017; Hernes et al., 2008), and dissolved black carbon (Stubbins et al., 2015; Wagner et al., 2015) during periods of high flow across diverse river systems. Pope, Sleepers, and Passumpsic exhibit the highest H/C ratios at storm onset (Figure 7). Abundance-weighted average H/C ratios drop quickly after storm onset and continue to decrease steadily through peak discharge and along the falling limb of the hydrograph (Figure 7). This shift from high to low H/C along the hydrograph further indicates an increase in the overall degree of aromaticity of DOM exported during the storm event. Since DOC concentrations and humic-like FDOM signals are also elevated during high discharge (Figure 2), we can conclude that aromatic carbon concentrations and export are also highest during peak discharge and hydrograph recession.

The low number of discrete samples collected and lack of prestorm/poststorm baseflow and end-member (soil water, groundwater, etc.) samples prevented statistically robust linkages to be made between DOM sources and hydrological pathways. However, variations in FDOM (Figure 2) indicated potential shifts in riverine DOM sources during the storm event. The DOM molecular formula signature also shifted from being more enriched in aliphatics to being more enriched in aromatics between storm onset and peak discharge. This change in DOM composition is driven by the timing of different DOM sources reaching the stream. Classical interpretations of hysteresis suggest that groundwater arrives first, surface flow second, and soil flow last due to the speed at which water movement through these flow paths can respond to

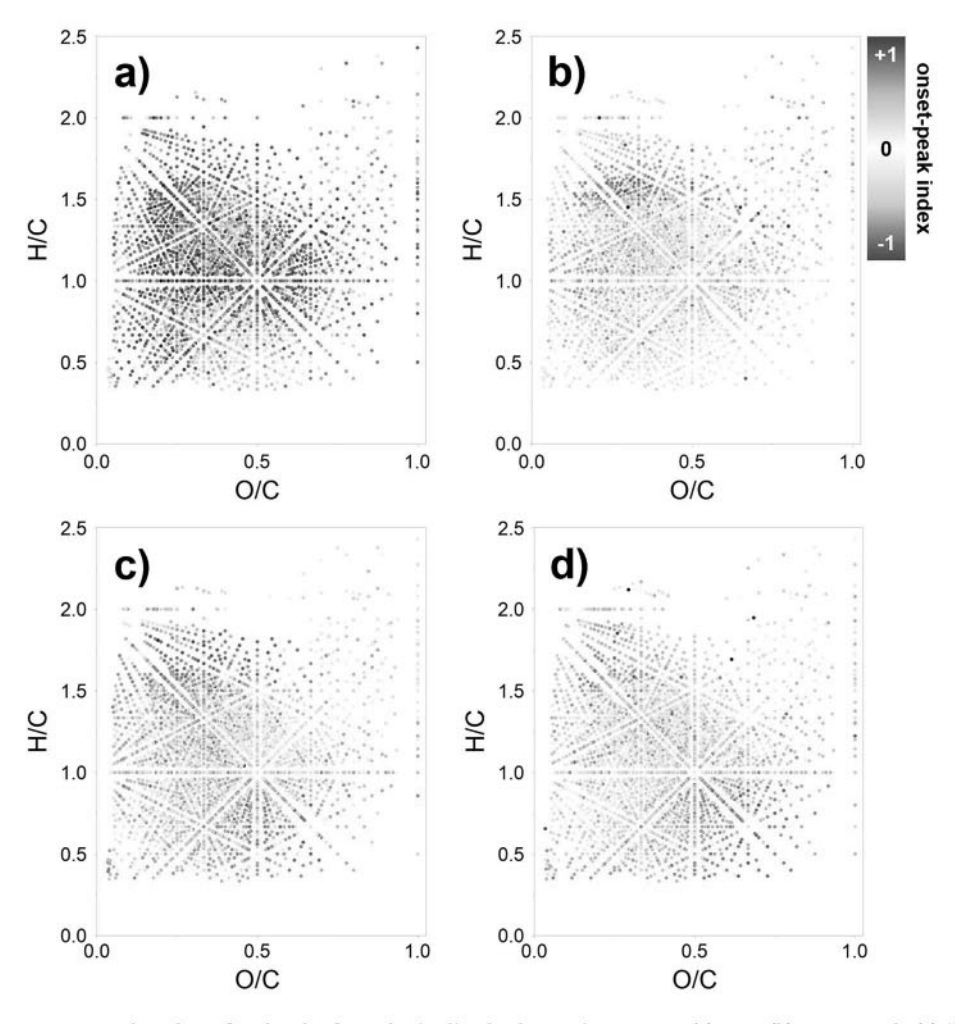


Figure 8. Van Krevelen plots of molecular formulas in dissolved organic matter at (a) W-9, (b) Pope Brook, (c) Sleepers River, and (d) Passumpsic River. Individual points are colored based upon the onset-peak index described in the text. The purple points represent formulas that were more abundant at storm onset. The green points represent formulas that were more abundant at peak discharge.

fresh rainfall (Evans & Davies, 1998). The quality of these end-members is then inferred from the timing of solute chemistry in the river. In the case of DOC, FDOM, and FT-ICRMS data here, such an interpretation suggests that groundwater has low FDOM and aliphatic-enriched DOC. This is consistent with what is known about groundwater chemistry, which generally has low DOC, low humic-like FDOM, and is enriched in aliphatic formulas, but depleted in aromatic formulas (Inamdar et al., 2011; Kellerman et al., 2018). As the storm progresses toward peak discharge, DOC, FDOM, and aromatic content increase with discharge but generally peak after peak discharge, leading to a counterclockwise hysteresis at our sites (Figures 3 and 6). Following the interpretation of hysteresis forwarded by Evans and Davies (1998), this implies that surface flow is enriched in DOC, FDOM, and aromatics compared to groundwater, but the late arriving soil flow paths are further enriched in each of these parameters compared to surface flow.

DOC and FDOM hysteresis patterns for the current storm event are similar to those previously recorded by Shanley et al. (2015). Using a multitracer approach, they showed the delayed peak in aromatic DOM to be driven by the flow of water through distal organic soil horizons (Shanley et al., 2015). Highly colored (aromatic) DOM is also sourced from the leaching of fresh leaf litter during storms that occur after leaf drop in autumn (Shanley et al., 2015). In the current study, samples were collected during a storm, which occurred in the weeks following leaf drop in northern Vermont (USA); therefore, the polyphenolic, aromatic DOM signature evident at peak discharge (Figure 9b) could be derived from the solubilization of this freshly deposited organic material. The molecular hysteresis described here lays the groundwork for the

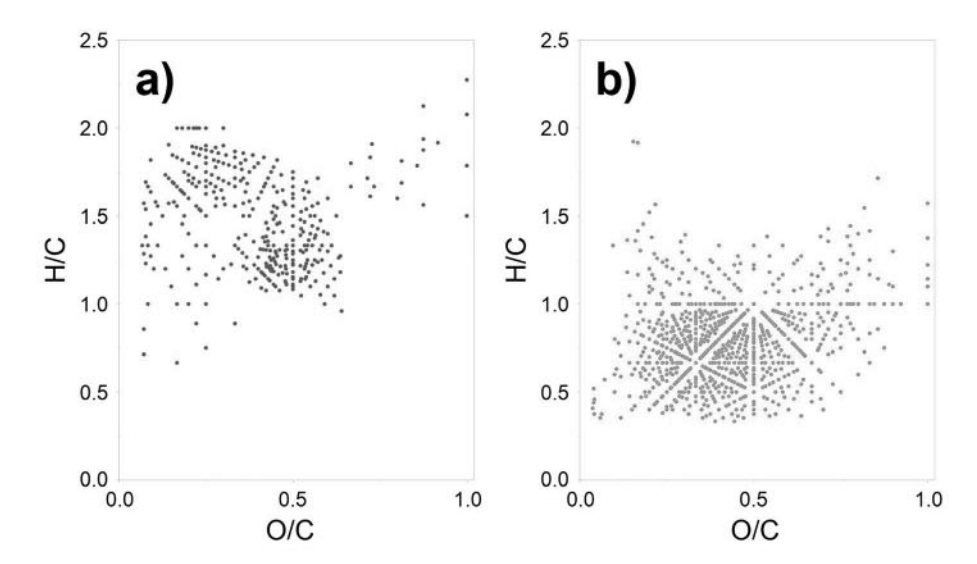


Figure 9. Van Krevelen plots of molecular formulas, which were consistently enriched at (a) storm onset (onset-peak index >1) and (b) peak discharge (onset-peak index <1) across all sampling sites (W-9, Pope, Sleepers, and Passumpsic).

identification of molecular formulas or compounds that are mobilized in-stream at different points across the hydrograph. However, further work is needed to assess between-storm and seasonal variations in molecular composition and determine which groups of compounds are consistently present/absent or enriched/depleted across different seasons and storm sizes. Future studies that seek to investigate DOM molecular hysteresis should collect prestorm and poststorm baseflow samples to verify the unique presence of the group of aliphatic compounds at storm onset and to determine whether the molecular compositions of DOM during prestorm and poststorm baseflow are similar.

### 4.3. Molecular Hysteresis: Implications for Pulse-Shunt and Downstream Biogeochemistry

The river continuum concept hypothesizes that the molecular diversity of DOM is highest in the headwaters and decreases with increasing stream order (Vannote et al., 1980). The high degree of molecular diversity proposed for riverine headwaters is driven by the heterogeneity of DOM source and the varied spatiotemporal delivery of DOM to the stream channel (Creed et al., 2015). In higher order streams, molecular diversity is hypothesized to be reduced by the biogeochemical processing of DOM as it transits downstream (Creed et al., 2015). In support of the river continuum concept, Mosher et al. (2015) showed first-order streams to contain DOM with the highest molecular diversity (highest number of unique molecular formulas) when sampled under baseflow conditions. However, in the current study no molecular formulas were found to be unique to any stream order during the storm event and the variation at a single site (i.e., stream order) across the storm was greater than variation across stream orders. Furthermore, molecular hysteresis patterns were found to be quite similar across all stream orders (Figures 8 and 9). This indicates that despite variations in catchment landscape and basin area, event discharge disrupts the downstream gradient in DOM molecular composition that is evident at baseflow (Mosher et al., 2015). The homogenization of DOM composition across stream orders during an event provides further evidence to support the pulseshunt concept, whereby rivers are converted from active to passive pipes at high flow, transporting fresh, terrestrial DOM further downstream (Raymond et al., 2016). The flushing of terrestrial DOM during storm events appears to shunt diverse DOM downstream and could relocate biogeochemical hotspots for DOM processing from the upper to the lower reaches of the watershed.

Hydrological events increase the percentage and flux of biologically available DOM in rivers with forested watersheds (Wilson et al., 2013). In the Yukon River, the proportion of biolabile DOC was found to be highest on the rising limb of the hydrograph (Wickland et al., 2012). The group of compounds preferentially mobilized during storm onset (Figure 9a) share similar molecular characteristics as formulas, which have been shown to be highly biolabile in permafrost (Spencer et al., 2015) and forested stream DOM (Kim et al., 2006). The prevalence of potentially biolabile molecules on the rising limb of the hydrograph across all stream orders indicates that these biogeochemically reactive compounds are shunted further through



the river network during periods of high discharge and could serve as a fresh carbon subsidy to microbial communities present in higher stream orders. However, the observed trends in FT-ICRMS data alone cannot fully support this hypothesis. Therefore, biolability experiments are needed to determine when biologically available DOM is most prevalent during storm events in the Passumpsic River watershed. The event-driven export of these compounds could propagate a surge in labile DOM and associated microbial activity at the leading edge of storm waters passing through a river network.

At and after peak discharge, DOM was enriched in aromatic molecular formulas (Figure 9b). Aromatic formulas tend to persist during water column biodegradation experiments (Spencer et al., 2015) but are preferentially degraded by sunlight (Stubbins et al., 2010, 2017). Therefore, photochemistry may control the fate of organics transported during pulse-shunt. However, during flood events several factors may limit the potential for photochemistry to occur in stream. First, during high discharge DOM residence times decrease, reducing the opportunity for photochemical reactions to occur. Second, at peak discharge, high turbidity would reduce the proportion of light absorbed by DOM (Figure S1). Finally, increased color and aromaticity of DOM indicates increased light absorbance of DOM during hydrograph recession (Figures 3 and 7). Enhanced DOM absorbance would result in DOM self-shading during storm events. If we assume light flux remains constant during a storm event, but DOM residence time decreases, turbidity increases, and DOM absorbance increases, then the number of photons per aromatic molecule in the water column decreases. A reduction in photons per aromatic molecule should promote the survival and transport of potentially photoreactive DOM molecules from rivers to the coast. Studies in various fluvial systems note that the export of aromatic-rich organics to the ocean increases during high discharge events (Spencer et al., 2008, 2013). In these cases, the pulse-shunt relocates the area for terrigenous DOM processing from the fluvial system to the coastal ocean.

### 5. Conclusions

Ultrahigh-resolution mass spectral analysis (FT-ICRMS) revealed molecular hysteresis of DOM within a forested New England watershed. At storm onset, DOM was enriched in aliphatic compounds, compared to peak discharge, when condensed aromatic and polyphenolic compounds were most prevalent. The observation of similar molecular hysteretic trends across stream orders within the nested catchment provides support for the pulse-shunt concept, in which fresh, unaltered, terrestrial DOM is quickly transported downstream during storm events, or other periods of high discharge. The biogeochemical effects of the short-term mobilization of reactive terrestrial DOM to the river main stem and coastal margins have yet to be fully realized. However, the rapid delivery of riverine DOM downstream could ultimately fuel transient biogeochemical hotspots at higher stream orders or within the coastal zone. The current study provides a view into molecular-level hysteretic changes in DOM, which is not offered by measurements of bulk DOC or by optical spectroscopic techniques. Further work on molecular hysteresis would benefit from the collection of discrete samples at higher resolution across the hydrograph, capturing true prestorm and poststorm baseflow samples, and obtaining possible end-member DOM samples (groundwater, soil water, etc.) to better constrain sources that contribute to the DOM molecular formula signature during storm events. For example, by comparing DOC, FDOM, and molecular formula signatures of hydrologic end-members (groundwater, surface water, and soil water) to signatures at different points along the hydrograph, we could infer changes in flow paths and sources of DOM during storm events.

# Acknowledgments This work is supported by NSF Macrosystems Biology awards 1824613 and 1340749. L. Zhu and Z. Fang are thanked for their assistance with DOM extractions. Any use of trade, firm, or product names is for descriptive purposes only and does not imply endorsement by the U.S. Government. Additional methods and data can be

found in the supporting information.

### References

- Buffam, I., Galloway, J. N., Blum, L. K., & McGlathery, K. J. (2001). A stormflow/baseflow comparison of dissolved organic matter concentrations and bioavailability in an Appalachian stream. Biogeochemistry, 53(3), 269–306. https://doi.org/10.1023/A:1010643432253
  Butturini, A., Alvarez, M., Bernal, S., Vazquez, E., & Sabater, F. (2008). Diversity and temporal sequences of forms of DOC and NO<sub>3</sub>-discharge responses in an intermittent stream: Predictable or random succession? Journal of Geophysical Research, 113, G03016. https://doi.org/10.1029/2008JG000721
- Butturini, A., Gallart, F., Latron, J., Vazquez, E., & Sabater, F. (2006). Cross-site comparison of variability of DOC and nitrate c-q hysteresis during the autumn-winter period in three Mediterranean headwater streams: A synthetic approach. *Biogeochemistry*, 77(3), 327–349. https://doi.org/10.1007/s10533-005-0711-7
- Creed, I. F., McKnight, D. M., Pellerin, B. A., Green, M. B., Bergamaschi, B. A., Aiken, G. R., et al. (2015). The river as a chemostat: Fresh perspectives on dissolved organic matter flowing down the river continuum. Canadian Journal of Fisheries and Aquatic Sciences, 72(8), 1272–1285. https://doi.org/10.1139/cifas-2014-0400
- Dhillon, G. S., & Inamdar, S. (2014). Storm event patterns of particulate organic carbon (POC) for large storms and differences with dissolved organic carbon (DOC). Biogeochemistry, 118(1-3), 61–81. https://doi.org/10.1007/s10533-013-9905-6

- Dittmar, T., Koch, B., Hertkorn, N., & Kattner, G. (2008). A simple and efficient method for the solid-phase extraction of dissolved organic matter (SPE-DOM) from seawater. Limnology and Oceanography: Methods, 6(6), 230-235. https://doi.org/10.4319/lom.2008.6.230.
- Dittmar, T., & Koch, B. P. (2006). Thermogenic organic matter dissolved in the abyssal ocean. *Marine Chemistry*, 102(3-4), 208–217. https://doi.org/10.1016/j.marchem.2006.04.003
- Downing, B. D., Pellerin, B. A., Bergamaschi, B. A., Saraceno, J. F., & Kraus, T. E. C. (2012). Seeing the light: The effects of particles, dissolved materials, and temperature on in situ measurements of DOM fluorescence in rivers and streams. *Limnology and Oceanography: Methods*, 10(10), 767–775. https://doi.org/10.4319/lom.2012.10.767
- Eckard, R. S., Pellerin, B. A., Bergamaschi, B. A., Bachand, P. A. M., Bachand, S. M., Spencer, R. G. M., & Hernes, P. J. (2017). Dissolved organic matter compositional change and biolability during two storm runoff events in a small agricultural watershed. *Journal of Geophysical Research: Biogeosciences*, 122, 2634–2650. https://doi.org/10.1002/2017JG003935
- Evans, C., & Davies, T. D. (1998). Causes of concentration/discharge hysteresis and its potential as a tool for analysis of episode hydrochemistry. Water Resources Research, 34(1), 129-137. https://doi.org/10.1029/97WR01881
- Hernes, P. J., Spencer, R. G. M., Dyda, R. Y., Pellerin, B. A., Bachand, P. A. M., & Bergamaschi, B. A. (2008). The role of hydrologic regimes on dissolved organic carbon composition in an agricultural watershed. Geochimica et Cosmochimica Acta, 72(21), 5266–5277. https://doi. org/10.1016/j.gca.2008.07.031
- Hertkorn, N., Benner, R., Frommberger, M., Schmitt-Kopplin, P., Witt, M., Kaiser, K., et al. (2006). Characterization of a major refractory component of marine dissolved organic matter. Geochimica et Cosmochimica Acta, 70(12), 2990–3010. https://doi.org/10.1016/j.gca.2006.03.021
- Hood, E., Gooseff, M. N., & Johnson, S. L. (2006). Changes in the character of stream water dissolved organic carbon during flushing in three small watersheds Oregon. *Journal of Geophysical Research*, 111, G02011. https://doi.org/10.1029/2005JG000082
- House, W. A., & Warwick, M. S. (1998). Hysteresis of the solute concentration/discharge relationship in rivers during storms. Water Research, 32(8), 2279–2290. https://doi.org/10.1016/S0043-1354(97)00473-9
- Inamdar, S., O'Leary, N., Mitchell, M., & Riley, J. (2006). The impact of storm events on solute exports from a glaciated forested watershed in western New York, USA. Hydrological Processes, 20(16), 3423-3439. https://doi.org/10.1002/hyp.6141
- Inamdar, S., Singh, S., Dutta, S., Levia, D., Mitchell, M., Scott, D., et al. (2011). Fluorescence characteristics and sources of dissolved organic matter for stream water during storm events in a forested mid-Atlantic watershed. *Journal of Geophysical Research*, 116, G03043. https://doi.org/10.1029/2011JG001735
- Jaffé, R., Yamashita, Y., Maie, N., Cooper, W. T., Dittmar, T., Dodds, W. K., et al. (2012). Dissolved organic matter in headwater streams: Compositional variability across climatic regions of North America. Geochimica et Cosmochimica Acta, 94, 95–108. https://doi.org/ 10.1016/j.gca.2012.06.031
- Kellerman, A. M., Guillemette, F., Podgorski, D. G., Aiken, G. R., Butler, K. D., & Spencer, R. G. M. (2018). Unifying concepts linking dissolved organic matter composition to persistence in aquatic ecosystems. *Environmental Science and Technology*, 52(5), 2538–2548. https://doi.org/10.1021/acs.est.7b05513
- Kim, S., Kaplan, L. A., & Hatcher, P. G. (2006). Biodegradable dissolved organic matter in a temperate and a tropical storm determined from ultra-high resolution mass spectrometry. *Limnology and Oceanography*, 51(2), 1054–1063. https://doi.org/10.4319/lo.2006.51.2.1054
- Kim, S., Kramer, R. W., & Hatcher, P. G. (2003). Graphical method for analysis of ultrahigh-resolution broadband mass spectra of natural organic matter, the van Krevelen diagram. Analytical Chemistry, 75(20), 5336-5344. https://doi.org/10.1021/ac034415p
- Koch, B. P., & Dittmar, T. (2006). From mass to structure: An aromaticity index for high-resolution mass data of natural organic matter. Rapid Communications in Mass Spectrometry, 20(5), 926–932. https://doi.org/10.1002/rcm.2386
- Koch, B. P., & Dittmar, T. (2016). From mass to structure: An aromaticity index for high-resolution mass data of natural organic matter. Rapid Communications in Mass Spectrometry, 30(1), 250. https://doi.org/10.1002/rcm.7433
- Koch, B. P., Dittmar, T., Witt, M., & Kattner, G. (2007). Fundamentals of molecular formula assignment to ultrahigh resolution mass data of natural organic matter. Analytical Chemistry, 79(4), 1758–1763. https://doi.org/10.1021/ac061949s
- Kujawinski, E. B. (2002). Electrospray ionization Fourier transform ion cyclotron resonance mass spectrometry (ESI FT-ICR MS): Characterization of complex environmental mixtures. Environmental Forensics, 3(3), 207–216. https://doi.org/10.1080/713848382
- Kujawinski, E. B., Freitas, M. A., Zang, X., Hatcher, P. G., Green-Church, K. B., & Jones, B. (2002). The application of electrospray ionization mass spectrometry (ESI MS) to the structural characterization of natural organic matter. *Organic Geochemistry*, 33(3), 171–180. https://doi.org/10.1016/S0146-6380(01)00149-8
- Lechtenfeld, O. J., Kattner, G., Flerus, R., McCallister, S. L., Schmitt-Kopplin, P., & Koch, B. P. (2014). Molecular transformation and degradation of refractory dissolved organic matter in the Atlantic and Southern Ocean. Geochimica et Cosmochimica Acta, 126, 321–337. https://doi.org/10.1016/j.gca.2013.11.009
- Lloyd, C. E. M., Freer, J. E., Johnes, P. J., & Collins, A. L. (2016). Technical note: Testing an improved index for analyzing storm discharge-concentration hysteresis. Hydrology and Earth System Sciences, 20(2), 625–632. https://doi.org/10.5194/hess-20-625-2016
- Mosher, J. J., Kaplan, L. A., Podgorski, D. C., Mckenna, A. M., & Marshall, A. G. (2015). Longitudinal shifts in dissolved organic matter chemogeography and chemodiversity within headwater streams: A river continuum reprise. *Biogeochemistry*, 124(1-3), 371–385. https://doi.org/10.1007/s10533-015-0103-6
- Pellerin, B. A., Saraceno, J. F., Shanley, J. B., Sebestyen, S. D., Aiken, G. R., Wollheim, W. M., & Bergamaschi, B. A. (2012). Taking the pulse of snowmelt: In situ sensors reveal seasonal, event and diurnal patterns of nitrate and dissolved organic matter variability in an upland forest stream. Biogeochemistry, 108(1-3), 183–198. https://doi.org/10.1007/s10533-011-9589-8
- Radtke, D. B., Davis, J. V., & Wilde, F. D. (2005). Specific electrical conductance: US Geological Survey techniques of water resources investigations (Book 9, chap. A6., sec. 6.3). Geological Survey (US).
- Raymond, P. A., & Saiers, J. E. (2010). Event controlled DOC export from forested watersheds. Biogeochemistry, 100(1-3), 197–209. https://doi.org/10.1007/s10533-010-9416-7
- Raymond, P. A., Saiers, J. E., & Sobczak, W. V. (2016). Hydrological and biogeochemical controls on watershed dissolved organic matter export: Pulse-shunt concept. Ecology, 97(1), 5–16. https://doi.org/10.1890/14-1684.1
- Riedel, T., & Dittmar, T. (2014). A method detection limit for the analysis of natural organic matter via Fourier transform ion cyclotron resonance mass spectrometry. Analyical Chemistry, 86(16), 8376–8382. https://doi.org/10.1021/ac501946m
- Šantl-Temkiv, T., Finster, K., Dittmar, T., Hansen, B. M., Thyrhaug, R., Nielsen, N. W., & Karlson, U. G. (2013). Hailstones: A window into the microbial and chemical inventory of a storm cloud. PLoS ONE, 8(1), e53550. https://doi.org/10.1371/journal.pone.0053550
- Shanley, J. B., Sebestyen, S. D., McDonnell, J. J., McGlynn, B. L., & Dunne, T. (2015). Water's Way at Sleepers River watershed— Revisiting flow generation in a post-glacial landscape, Vermont USA. *Hydrological Processes*, 29(16), 3447–3459. https://doi.org/10.1002/hyp.10377

- Singer, G. A., Fasching, C., Wilhelm, L., Niggemann, J., Steier, P., Dittmar, T., & Battin, T. J. (2012). Biogeochemically diverse organic matter in Alpine glaciers and its downstream fate. *Nature Geoscience*, 5(10), 710–714. https://doi.org/10.1038/ngeo1581
- Sleighter, R. L., & Hatcher, P. G. (2007). The application of electrospray ionization coupled to ultrahigh resolution mass spectrometry for the molecular characterization of natural organic matter. *Journal of Mass Spectrometry*, 42(5), 559–574. https://doi.org/10.1002/jms.1221
- Spencer, R. G., Aiken, G. R., Wickland, K. P., Striegl, R. G., & Hernes, P. J. (2008). Seasonal and spatial variability in dissolved organic matter quantity and composition from the Yukon River basin Alaska. Global Biogeochemical Cycles, 22, GB4002. https://doi.org/ 10.1029/2008GB003231
- Spencer, R. G. M., Mann, P. J., Dittmar, T., Eglinton, T. I., McIntyre, C., Holmes, R. M., et al. (2015). Detecting the signature of permafrost thaw in Arctic rivers. *Geophysical Research Letters*, 42, 2830–2835. https://doi.org/10.1002/2015GL063498
- Spencer, R. G. M., Stubbins, A. & Gaillardet, J. (2013). Geochemistry of the Congo River, estuary and plume. Biogeochemical dynamics at large river-coastal interfaces: Linkages with Global Climate Change (pp. 554–584).
- Stubbins, A., & Dittmar, T. (2012). Low volume quantification of dissolved organic carbon and dissolved nitrogen. Limnology and Oceanography: Methods, 10(5), 347–352. https://doi.org/10.4319/lom.2012.10.347
- Stubbins, A., Lapierre, J. F., Berggren, M., Prairie, Y. T., Dittmar, T., & del Gorgio, P. A. (2014). What's in an EEM? Molecular signatures associated with dissolved organic fluorescence in boreal Canada. Environmental Science and Technology, 48(18), 10,598–10,606. https://doi.org/10.1021/es502086e
- Stubbins, A., Mann, P. J., Powers, L., Bittar, T. B., Dittmar, T., McIntyre, C. P., et al. (2017). Low photolability of yedoma permafrost dissolved organic carbon. *Journal of Geophysical Research: Biogeosciences*, 122, 200–211. https://doi.org/10.1002/2016JG003688
- Stubbins, A., Spencer, R. G. M., Chen, H., Hatcher, P. G., Mopper, K., Hernes, P. J., et al. (2010). Illuminated darkness: Molecular signatures of Congo River dissolved organic matter and its photochemical alteration as revealed by ultrahigh precision mass spectrometry. Limnology and Oceanography, 55(4), 1467–1477. https://doi.org/10.4319/lo.2010.55.4.1467
- Stubbins, A., Spencer, R. G. M., Mann, P. J., Holmes, R. M., McClelland, J. W., Niggemann, J., & Dittmar, T. (2015). Utilizing colored dissolved organic matter to derive dissolved black carbon export by arctic rivers. *Frontiers in Earth Science*, 3, 63. https://doi.org/10.3389/ feart.2015.00063
- Vannote, R. L., Minshall, G. W., Cummins, K. W., Sedell, J. R., & Cushing, C. E. (1980). River continuum concept. Canadian Journal of Fisheries and Aquatic Sciences, 37(1), 130–137. https://doi.org/10.1139/f80-017
- Vaughan, M. C. H., Bowden, W. B., Shanley, J. B., Vermilyea, A., Sleeper, R., Gold, A. J., et al. (2017). High-frequency dissolved organic carbon and nitrate measurements reveal differences in storm hysteresis and loading in relation to land cover and seasonality. Water Resources Research, 53, 5345–5363. https://doi.org/10.1002/2017WR020491
- Vidon, P., Wagner, L. E., & Soyeux, E. (2008). Changes in the character of DOC in streams during storms in two Midwestern watersheds with contrasting land uses. Biogeochemistry, 88(3), 257–270. https://doi.org/10.1007/s10533-008-9207-6
- Wagner, S., Cawley, K. M., Rosario-Ortiz, F. L., & Jaffé, R. (2015). In-stream sources and links between particulate and dissolved black carbon following a wildfire. Biogeochemistry, 124(1-3), 145–161. https://doi.org/10.1007/s10533-015-0088-1
- Wagner, S., Riedel, T., Niggemann, J., Vahatalo, A. V., Dittmar, T., & Jaffé, R. (2015). Linking the molecular signature of heteroatomic dissolved organic matter to watershed characteristics in world rivers. Environmental Science and Technology, 49(23), 13,798–13,806. https://doi.org/10.1021/acs.est.5b00525
- Wickland, K. P., Aiken, G. R., Butler, K., Dornblaser, M. M., Spencer, R. G. M., & Striegl, R. G. (2012). Biodegradability of dissolved organic carbon in the Yukon River and its tributaries: Seasonality and importance of inorganic nitrogen. Global Biogeochemical Cycles, 26, GB0E03. https://doi.org/10.1029/2012GB004342
- Wilson, H. F., Saiers, J. E., Raymond, P. A., & Sobczak, V. W. (2013). Hydrologic drivers and seasonality of dissolved organic carbon concentration, nitrogen content, bioavailability, and export in a forested New England stream. *Ecosystems*, 16(4), 604–616. https://doi.org/10.1007/s10021-013-9635-6
- Yoon, B., & Raymond, P. A. (2012). Dissolved organic matter export from a forested watershed during Hurricane Irene. Geophysical Research Letters, 39, L18402. https://doi.org/10.1029/2012GL052785
- Zark, M., Christoffers, J., & Dittmar, T. (2017). Molecular properties of deep-sea dissolved organic matter are predictable by the central limit theorem: Evidence from tandem FT-ICR-MS. Marine Chemistry, 191, 9-15. https://doi.org/10.1016/j.marchem.2017.02.005